Microchimica Acta
https://doi.org/10.1007/s00604-018-3194-7

ORIGINAL PAPER

Amplification-free and direct fluorometric determination of telomerase activity in cell lysates using chimeric DNA-templated silver nanoclusters

Shi Ting Lee[1] · Ruman Rahman[2] · Kasturi Muthoosamy[3] · Nur Aliana Hidayah Mohamed[4] · XiaoDi Su[5,6,7] · Saad Tayyab[8] · Siu Yee New[1]

Received: 6 September 2018 / Accepted: 20 December 2018

Abstract

A fluorogenic probe has been developed for determination of telomerase activity using chimeric DNA-templated silver nanoclusters (AgNCs). The formation of AgNCs was investigated before (route A) and after (route B) telomerase elongation reaction. Both routes caused selective quenching of the yellow emission of the AgNCs (best measured at excitation/emission wavelength of 470/557 nm) in telomerase-positive samples. The quenching mechanism was studied using synthetically elongated DNA to mimic the telomerase-catalyzed elongation. The findings show that quenching is due to the formation of parallel *G*-quadruplexes with a *–TTA–* loop in the telomerase elongated products. The assay was validated using different cancer cell extracts, with intra- and interassay coefficients of variations of <9.8%. The limits of detection for MCF7, RPMI 2650 and HT29 cell lines are 15, 22 and 39 cells/μL. This represents a distinct improvement over the existing telomeric repeat amplification protocol (TRAP) assay in terms of time, sensitivity and cost.

Keywords Cancer probe · AgNCs · Biomarker · Biosensor · TRAP · G-quadruplex · Telomers · MCF7 · HT29 · RPMI 2650

Introduction

Telomerase is a ribonucleoprotein that plays an important role in maintaining chromosome ends and preventing them from degradation, recombination and end-to-end fusion [1–4]. Structurally, telomerase consists of (1) a recognition site, i.e. an RNA template that binds to telomeric repeats in situ and telomerase substrate (TS) primer in vitro, and (2) a catalytic site, i.e. telomerase elongated reverse transcriptase (TERT) that adds repetitive *TTAGGG* nucleotides onto the 3′-end of telomeres in situ or the TS primer in vitro [5, 6]. While telomerase is absent in human somatic cells, it is highly expressed in 85% of cancer cells [7], demonstrating its potential role as a biomarker for cancer detection and prognosis.

The gold standard assay to detect telomerase in vitro is known as telomeric repeat amplification protocol (TRAP) [8]. However, TRAP assay often suffers from polymerase chain reaction (PCR) associated artifacts and is relatively time-consuming. Thus, several PCR-free measurement methods have been developed to detect crude telomerase extracts, which include electrochemical [9, 10], chemiluminescence [11, 12], colorimetric [13, 14] and fluorescence [15–20]. These methods are either clinically not

Electronic supplementary material The online version of this article (https://doi.org/10.1007/s00604-018-3194-7) contains supplementary material, which is available to authorized users.

✉ Siu Yee New
SiuYee.New@nottingham.edu.my

[1] School of Pharmacy, Faculty of Science, University of Nottingham Malaysia, Jalan Broga, 43500 Semenyih, Selangor, Malaysia

[2] Children's Brain Tumour Research Centre (CBTRC), School of Medicine, Queen's Medical Centre, University of Nottingham, Nottingham NG7 2UH, UK

[3] Nanotechnology and Advanced Materials (NATAM), Faculty of Engineering, University of Nottingham Malaysia, Jalan Broga, 43500 Semenyih, Selangor, Malaysia

[4] Centre of Clinical Science, Faculty of Dentistry, University of Technology MARA Sungai Buloh Campus, Jalan Hospital, 47000 Sungai Buloh, Selangor, Malaysia

[5] Institute of Materials Research and Engineering, 2 Fusionopolis Way, Singapore 138634, Singapore

[6] Department of Chemistry, National University of Singapore, 3 Science Drive 3, Singapore 117543, Singapore

[7] School of Science and Engineering, University of the Sunshine Coast, Locked Bag 4, Maroochydore DC, Queensland 4558, Australia

[8] Institute of Biological Sciences, Faculty of Science, University of Malaya, 50603 Kuala Lumpur, Malaysia

Published online: 09 January 2019

feasible or have restricted practical applicability. For instance, catalytic activity of enzymes used in chemiluminescence assays is sensitive to enzyme degradation and often limited due to embedment of activity centre in the macromolecules [21]. Hence the chemiluminescence often requires additional methods to enhance its operational stability and signal amplification, which subsequently increases the assay cost. Similarly, not only the dye-labeling in fluorescence methods increases production cost, the covalent attachment of the reporter molecules to the functional oligonucleotides may also affect the recognition event [22, 23]. In light of this, a new kind of fluorescent probe has been developed for direct detection of telomerase activity on cell lysates [24–26]. Li et al. [26] and Huang et al. [25] have recently reported on using DNA-templated silver nanoclusters (DNA-AgNCs) for direct detection on telomerase activity through fluorescence enhancement by guanine (*G*)-rich telomerase elongated product. Not only AgNCs are small in size (i.e. 2 nm in diameter), photostable and biocompatible, but the easy integration of this nanomaterial in DNA template has further added versatility in assay design.

While both aforementioned studies employed a NanoCluster beacon that promotes fluorescence enhancement via proximal *G*-rich repetitive sequence *TTAGGG* [27]; another simpler design can be achieved utilizing a chimeric DNA template, i.e. combining a AgNCs-nucleation sequence and functional DNA as a single-stranded DNA (ssDNA). This study stemmed from our previous findings on the use of chimeric DNA-templated AgNCs to detect adenosine [28]. To further leverage the chimeric design for telomerase detection, here we employ a DNA template called 'Ct_9TS' that consists of (i) Ct_9 as a known nucleation sequence of AgNCs [28] and (ii) TS primer for telomerase to bind and induce elongation reactions. The principle of detection is based on the fact that formation of telomerase-elongated products can affect stability of the neighboring AgNCs hosted in the same ssDNA. By measuring the emission intensity of AgNCs, one can selectively and quantitatively detect the telomerase activity in cell extracts, in a more rapid manner relative to conventional TRAP. To prove that AgNCs are confined in Ct_9, two different ways of detection were investigated: formation of AgNCs before and after telomerase elongation reaction, depicted as route A and route B, respectively, in Scheme 1. To support the working principle, a proof-of-concept study was conducted using synthetically elongated DNA, i.e. Ct_9TSR*n* (*n* = 3, 5 and 7), where *n* is the number of *TTAGGG* repeats.

Materials and methods

Materials

All desalted DNA oligonucleotides were purchased from Integrated DNA Technologies (IDT) (www.idtdna.com). Details of the DNA sequences are listed in Table 1. The chemicals used include silver nitrate, sodium borohydride and EDTA from Nacalai Tesque (www.apicalscientific.com); ammonium persulfate, *N,N,N′,N′*-tetramethylethane-1,2-diamine, magnesium chloride, potassium chloride and boric acid from R&M Chemicals (www.evergainful.com.my); 40% bis-acryamide and acrylamide solution (29:1), Tris, deoxyribonucleotide triphosphate, Taq buffer and Taq DNA polymerase from 1st Base (www.apicalscientific.com); ethylene glycol-bis(2-aminoethylether)-*N,N,N′,N′*-tetraacetic acid (EGTA), hydrochloric acid and phosphate buffered saline (PBS) pellets from Sigma Aldrich (www.sigmaaldrich.com); 1X CHAPS lysis buffer (0.5% CHAPS, 10 mM Tris-HCl, pH 7.5, 1 mM $MgCl_2$, 1 mM EGTA, 0.1 mM benzamidine, 5 mM 2-mercaptoethanol, 10% glycerol) from Merck (www.merckmillipore.com); Tween 20 from Systerm Chemicals (www.systermchemicals.com); SYBR Safe DNA Gel Stain from Invitrogen (www.thermofisher.com).

Instrumentation

Fluorescence measurements were conducted on a Hitachi F-7000 spectrofluorometer (Tokyo, Japan, www.mecomb.com) with a Xenon lamp as excitation source. The excitation and emission slit widths were both set at 10 nm, with photomultiplier tube voltage at 950 V and scanning speed of 2400 nm/min. UV-visible absorption spectra were acquired using an Epoch Microplate Reader (Biotek, U.S.A, www.biotek.com). High-resolution transmission electron microscopy (HR-TEM) images were acquired using FEI Tecnai G2-F20 operated at 200 kV with 0.2 nm resolution (www.fei.com). Circular dichroism (CD) measurements were conducted on a Jasco J-815 spectropolarimeter (Tokyo, Japan, www.jascoinc.com). Centrifugation was performed on a Beckman Coulter (California, U.S.A, www.beckmancoulter.com). Telomerase extension reaction was accomplished using a Biorad thermal cycler (California, USA, www.bio-rad.com). A ChemiDoc MP Imaging system (Bio-Rad, USA, www.bio-rad.com) was used to capture fluorescence images.

Telomerase extract preparation

Telomerase was extracted using the CHAPS method [19]. Briefly, cells were grown to 90% confluence and pelleted by centrifugation (60 x g for 5 min). The cell pellet was washed twice with 1x ice-cold PBS buffer to remove residual culture medium. Then, the pellet was resuspended in 200 μL 1X CHAPS lysis buffer by retropipeting five times before incubating in an ice bath for 30 min. The mixture was centrifuged at ~14,000 x g for 20 min at 4 °C. The concentration of total cellular

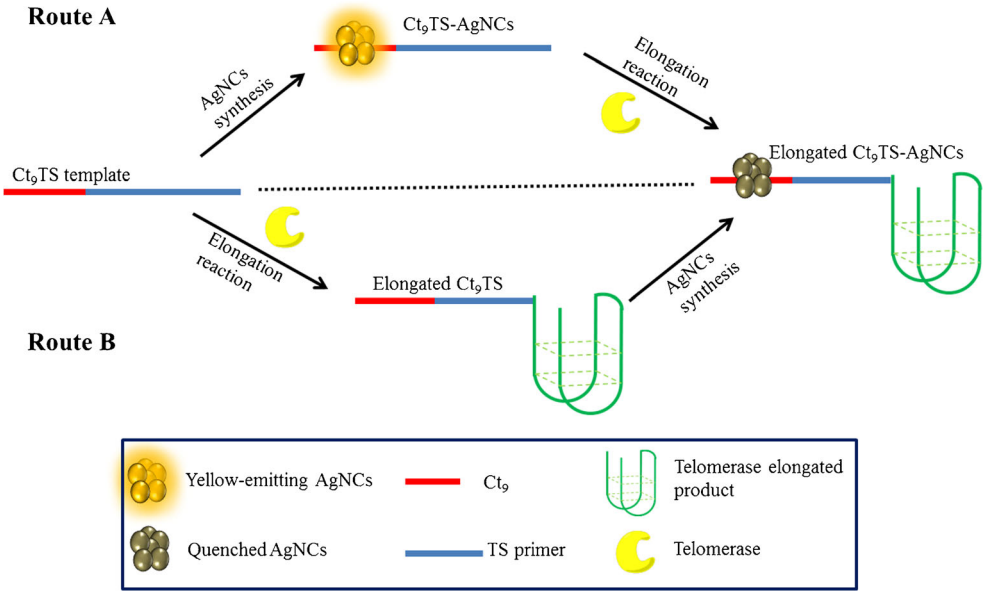

Scheme 1 Schematic presentation of two different ways to detect telomerase activity via formation of silver nanoclusters (AgNCs) before (route A) and after (route B) telomerase elongation reaction. The DNA template (Ct_9TS) used for AgNCs synthesis consists of nucleation sequence (Ct_9) and telomerase substrate (TS) primer

protein was determined using the Bradford assay, where 200 ng/μL corresponds to ≈1000 cells/μL. The supernatant containing telomerase was diluted using 1X CHAPS lysis buffer before used. Three different cancer cell types, namely, breast cancer (MCF7), colon cancer (HT29) and human nasal squamous cell carcinoma (RPMI 2650), were used.

Preparation of the AgNCs modified with Ct_9 nucleation sequence and the telomerase substrate (TS) primer (Ct9TS-AgNCs), and quantitation of telomerase activity

In general, AgNCs were prepared via one-pot synthesis and used without further purification. For telomerase detection, AgNCs were added to cell extracts via either route A or route B (as listed below), before subjected for fluorescent measurement using optimized excitation/emission wavelengths ($\lambda_{exc}/\lambda_{em}$ 470/557 nm). For negative controls, the telomerase extracts were heat-treated at 90 °C for 15 min. To clearly distinguish the changes of fluorescence intensities in the presence of telomerase, the relative fluorescence intensity (F_0 – F/ F_0) was calculated, where F and F_0 represent fluorescence intensity of AgNCs samples in the presence and absence of telomerase extracts, respectively. Unless otherwise stated, the concentration of as-synthesized DNA-AgNCs is referred to the final concentration of DNA used.

Route a

Preparation of AgNCs: 20 μL of 100 μM Ct_9TS primer was heated in a 90 °C water bath for 5 min and left for 10 min to cool down to room temperature. Next, 120 μL of telomerase extension buffer (*a.k.a.* TRAP buffer, containing 5 mM Tris-HCl, pH 8.3, 375 μM $MgCl_2$, 15.75 mM KCl, 0.0125% Tween 20 and 250 μM EGTA) and 30 μL of 300 μM $AgNO_3$ were added sequentially. The mixture was incubated in an ice bath for 15 min before 30 μL of 300 μM $NaBH_4$ was added. The resulting solution was further incubated for 1 h.

The as-prepared AgNCs were then mixed with 4 μL of telomerase extracts and 200 μM dNTP. The mixture was incubated at 30 °C for 1 h for telomerase elongation reaction.

Table 1 DNA templates used. Nucleation sequence (Ct_9), primers (TS and rTS) and synthetically elongated telomeric repeats are shown in red, black and blue, respectively

Name	Sequence (5′ → 3′)
Ct_9TS	ACC CAC CCA AAT CCG TCG AGC AGA GTT
Ct_9TSR3	ACC CAC CCA AAT CCG TCG AGC AGA GTT $(AGGGTT)_2$ AGG G
Ct_9TSR5	ACC CAC CCA AAT CCG TCG AGC AGA GTT $(AGGGTT)_4$ AGG G
Ct_9TSR7	ACC CAC CCA AAT CCG TCG AGC AGA GTT $(AGGGTT)_6$ AGG G
Reverse TS (rTS)	CTA ACC CTA ACC CTA ACC

Route B

10 μM of Ct_9TS primer was heat-treated and cooled as described above, before adding 4 μL of telomerase cell extract and 200 μM dNTP. The mixture was then incubated at 30 °C for 1 h for telomerase elongation reaction.

Next, the solution containing the telomerase elongated product was subjected to synthesis of DNA-AgNCs, by sequentially adding 120 μL of telomerase extension buffer, 30 μL of 300 μM $AgNO_3$ and 30 μL of 300 μM $NaBH_4$, as described above.

Proof-of-concept

Ct_9TSRn ($n = 3$, 5 and 7) was heat-treated at 90 °C for 5 min, then incubated at 30 °C for 1 h to mimic the condition of telomerase elongation reaction. Next, Ct_9TSRn was subjected to preparation of AgNCs under similar conditions as described in section "Route A". The resulting emission intensity was compared with that of Ct_9TS-AgNCs.

Conventional telomeric repeat amplification protocol (TRAP) assay

10 μL of elongated Ct_9TS produced through route B was added to 40 μL of solution contains 1X Taq buffer, 200 μM dNTP, 2.5 U of Taq DNA polymerase and 200 nM of reverse primer (rTS). PCR was conducted with the following program: 95 °C for 5 min; 33 cycles at 95 °C for 1 min; 60 °C for 1 min; 72 °C for 1 min; 72 °C for 5 min; 4 °C hold. 25 μL of the PCR product was then loaded onto 4.5% (*w*/*v*) agarose gel. The gel was run at room temperature for 100 min at 80 V and visualized by SYBR Safe DNA gel staining.

Results and discussion

Characterisation of the Ct_9TS-AgNCs

We first characterized Ct_9TS-templated AgNCs by means of HR-TEM, UV-vis and fluorescence spectroscopies (Fig. 1). The TEM micrographs depict formation of spherical Ct_9TS-AgNCs (~3 nm) and devoid of larger aggregates (Fig. 1a). Similar to other DNA-templated AgNCs studies, both UV-vis and fluorescence results of Ct_9TS-AgNCs reveal the presence of multiple emitting species [28–31] (Fig. 1b and c). The UV-vis peaks at 372 and 547 nm correspond to the absorptions of blue- and red-emitting AgNCs. The band in 400–500 nm region is broad, attributed to surface plasmon resonance of a trace amount of larger silver nanoparticles and absorption from the dominant yellow-emitting AgNCs [32]. Given the response of both blue- and red emitters towards telomerase elongation reaction is negligible ("Detection of telomerase activity in crude telomerase cell extract" section), the following studies focus only on the yellow species (optimized $\lambda_{ex}/\lambda_{em} = 470/557$ nm) that remains stable for at least 3 h (Fig. 2; Fig. S1). Notably, the emission properties of Ct_9TS-AgNCs is very similar to the previously reported study that used the same nucleation sequence, i.e. Ct_9 [28]. This implies that AgNCs are also selectively confined in Ct_9 in this context, while TS primer site remains intact for telomerase binding. However, the λ_{ex} of Ct_9TS-AgNCs is more blue-shifted as compared to that of the reported Ct_9Apta-AgNCs ($\lambda_{exc} = 490$ nm), possibly due to different multi-base bonding between AgNCs and the neighboring region (TS vs adenosine aptamer) [28].

Determination of telomerase activity in crude cell extract

The telomerase-elongated product, i.e. *G*-rich telomeric sequence, renders another possible region to host AgNCs [33] or may induce cluster-transfer [34]. To determine whether AgNCs preferably reside in the nucleation sequence (i.e. Ct_9) or in the elongated telomeric sequence, we examined the emission spectra of Ct_9TS-AgNCs before (route A) and after (route B) telomerase elongation reaction, using MCF7 as telomerase extract. The heat-treated MCF7 cells were used as negative controls, whereas 1X CHAPS lysis buffer served as a blank to represent the absence of cell extracts. We reasoned that if AgNCs are hosted in the elongated telomeric sequence, emission spectra collected from route A and route B will be different.

Interestingly, both routes produced the same types of emitters, implying neither cluster-transfer occurred [34] nor additional emitting-species was formed (Fig. 2) [35]. Among the three emitters (i.e. blue, yellow and red species), only the major yellow species shows obvious quenching in the presence of telomerase-positive samples (Fig. 2). Notwithstanding the quenching efficiency in route B is lower than that of route A. We reasoned that adding Ag^+ to the more complex synthesis medium in route B (i.e. containing telomerase cell extract, telomeric sequence and dNTP) has not only diminished the amount of AgNCs encapsulated in Ct_9 region, but the chelation of Ag^+ to *G* bases may also disrupt the *G*-quadruplexes of the elongated telomeric sequence [36]. Considering greater practicability of a ready-made probe in the clinical setting, route A was thus chosen for the subsequent studies.

As indicated from the above finding, Ct_9TS-AgNCs were not only stable in cell extracts, but also showed selective quenching in the presence of telomerase-positive samples.

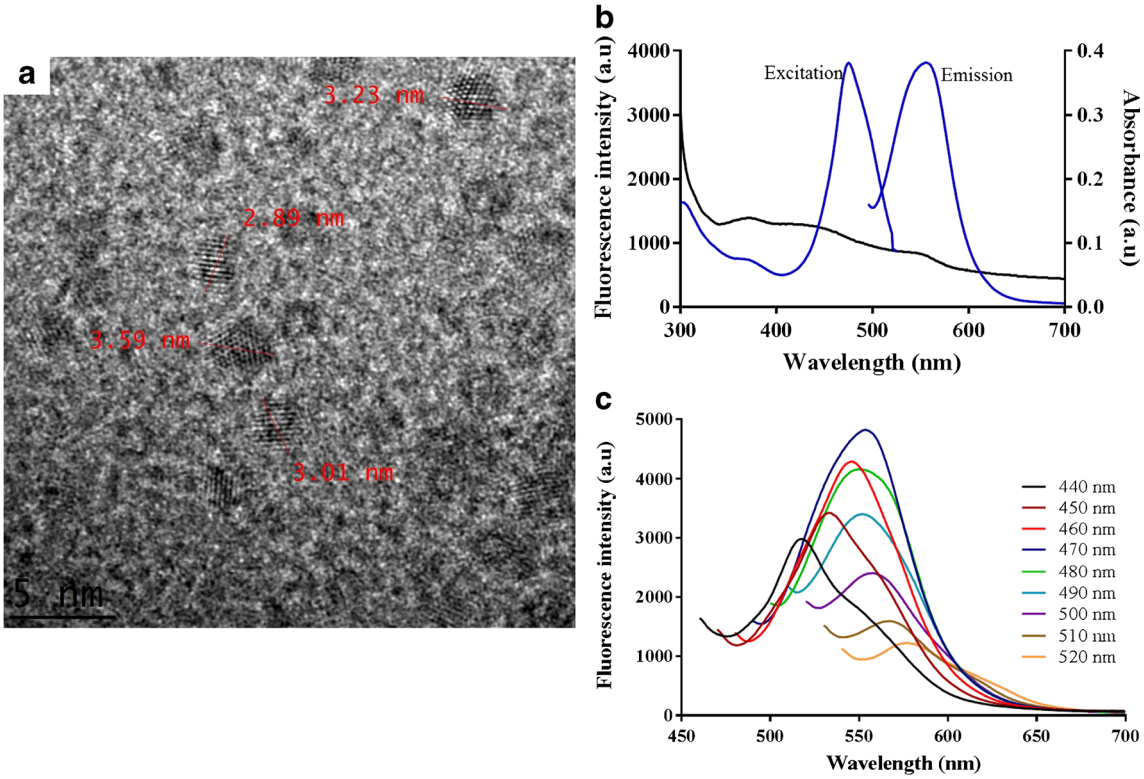

Fig. 1 **a** HR-TEM images of Ct_9TS-AgNCs. **b** UV-visible (black) and fluorescence spectra (blue) of Ct_9TS-AgNCs. Only fluorescence data of yellow emitters are shown ($\lambda_{ex}/\lambda_{em}$ = 470/557 nm). The concentration used was 450 nM. **c** Emission spectra of Ct_9TS-AgNCs excited from 440 to 520 nm

Control study proved that dNTP used in telomerase extension reaction does not contribute to the quenching of Ct_9TS-AgNCs, reinforcing the hypothesis that quenching is specific to telomerase elongated products (Fig. S2). To determine if Ct_9TS-AgNCs can be generally applied to different cancer cell lines, we further evaluated the assay on MCF7, HT29 and RPMI 2650 using different cell numbers. Fig. 3 shows that all telomerase-positive samples display distinctive

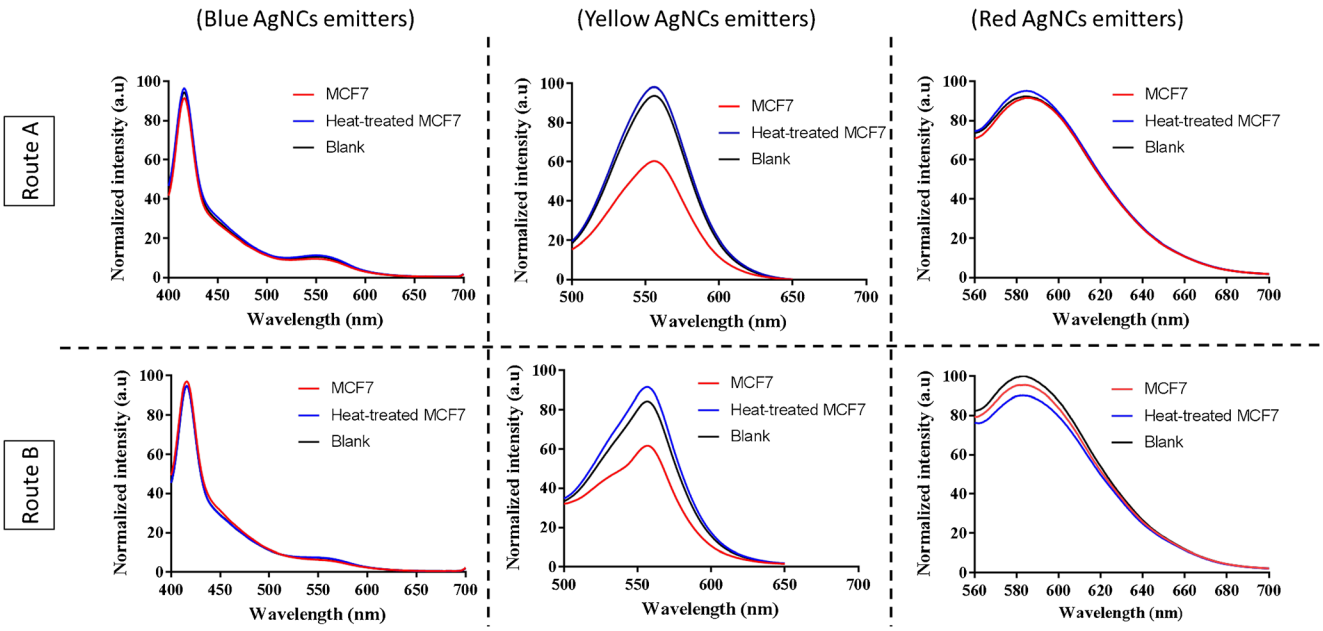

Fig. 2 Emission spectra of different Ct_9TS-AgNCs emitters prepared according to (**a**) route A and (**b**) route B using 250 MCF7 cells ($\lambda_{exc}/\lambda_{em}$of blue emitters = 365/416 nm; $\lambda_{exc}/\lambda_{em}$ of yellow emitters = 470/557 nm; $\lambda_{exc}/\lambda_{em}$ of red emitters = 540/585 nm)

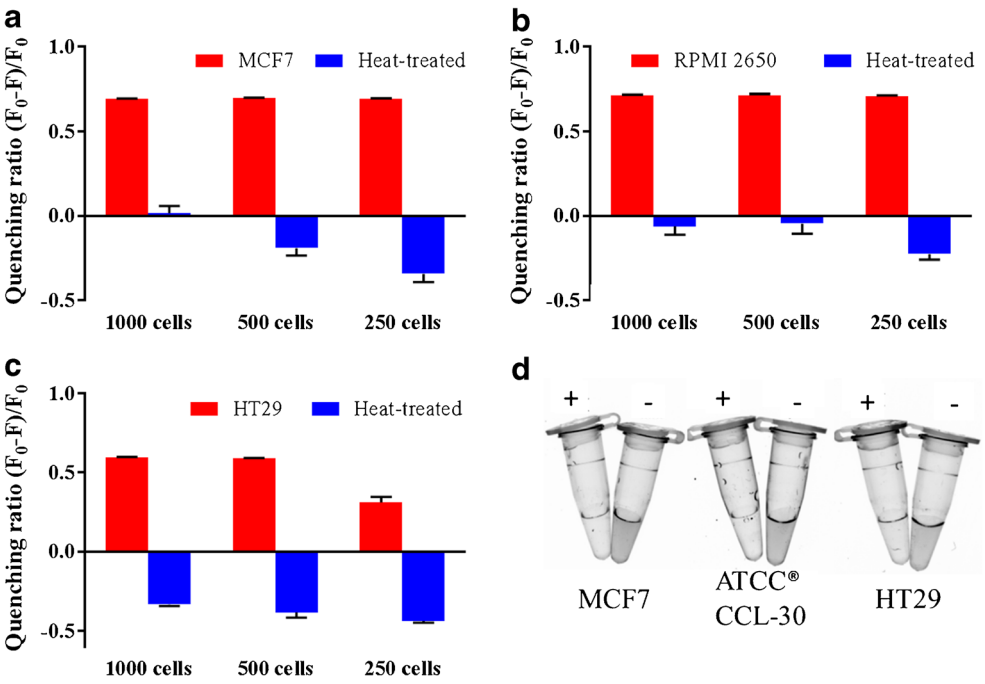

Fig. 3 Emission response of Ct_9TS-AgNCs at 1000, 500, and 250 cells of (**a**) MCF7, (**b**) RPMI 2650 and (**c**) HT29, with corresponding heat-denatured telomerase cell extracts as negative controls. (**d**) UV image of Ct_9TS-AgNCs in 250 cells of telomerase-positive (+) and -negative (−) samples. Error bars represent standard deviations from repeated independent measurements (n = 5)

fluorescence quenching from the negative controls. Results for precision, expressed as coefficients of variation (CV%), are 0.304–12.209% and 2.194–8.333% for intra- and interassay comparison (Table S1). These results suggest the reliability and selectivity of the assay over a range of oncological cell lines.

Interestingly, at the same number of cells, quenching ratios for RPMI 2650 and MCF7 are ~70%, comparatively higher than that of HT29, implying that the former two cell lines might have higher telomerase activity than HT29. As an independent confirmation of the telomerase activity trend, we performed the gold standard TRAP assay to crosscheck the findings. Based on the number and intensity of the telomerase-elongated PCR products, with reference to the 100 bp marker on an agarose gel (Fig. S3), an identical trend of telomerase activity was observed, with RPMI 2650 ≈ MCF7 > HT29. Notably, gel analysis often requires higher amounts of elongated DNA to visualize bands in the gels [25, 37], compared to our assay which needs only nanomolar concentrations of elongated Ct_9TS (Fig. S4). Furthermore, the difference between emission intensity of telomerase-positive and that of negative controls was achieved without any amplification steps, indicating the higher sensitivity of chimeric DNA-templated AgNCs towards subtle changes (i.e. elongated Ct_9TS-AgNCs) in the subject.

Next, to examine sensitivity, all three types of telomerase cell extracts were serially diluted and the emission response of AgNCs in each sample was plotted as a function of concentration (i.e. number of cells) (Fig. 4). We observed a good linear correlation in the range of 10 to 250 cells for MCF7; 25 to 250 cells for RPMI 2650; and 50 to 750 cells for HT29. The limits of detection (LOD) for MCF7, RPMI 2650 and HT29 are 15, 22 and 39 cells, respectively, calculated based on $3\sigma/m$, where σ is the standard deviation of the lowest concentration and m is the slope of the calibration curve. These results surpass the optimal sensitivity performance of conventional TRAP assay and other PCR-free methods, in the context of LOD and assay time (Table S2). Additionally, with AgNCs being label-free probes, the whole assay involves only simple mixing steps, thus enabling low-cost fabrication.

Proof-of-concept

To gain insight into how the telomerase-positive samples quench the fluorescence of Ct_9TS-AgNCs, we employed synthetically elongated DNA templates, i.e. Ct_9TSRn ($n = 3$, 5 and 7) to mimic different lengths of elongated products. As illustrated in Fig. 5a, the emission intensity of Ct_9TSR3-, Ct_9TSR5- and Ct_9TSR7-AgNCs decreased by ≥50% as compared to that of Ct_9TS-AgNCs without any telomeric sequence, which agrees well with the results in "Detection of telomerase activity in crude telomerase cell extract" section. The CD spectra of Ct_9TSRn templates and Ct_9TSRn-AgNCs prepared in TRAP buffer reveal the presence of parallel *G*-quadruplex structures (Fig. 5c and d).

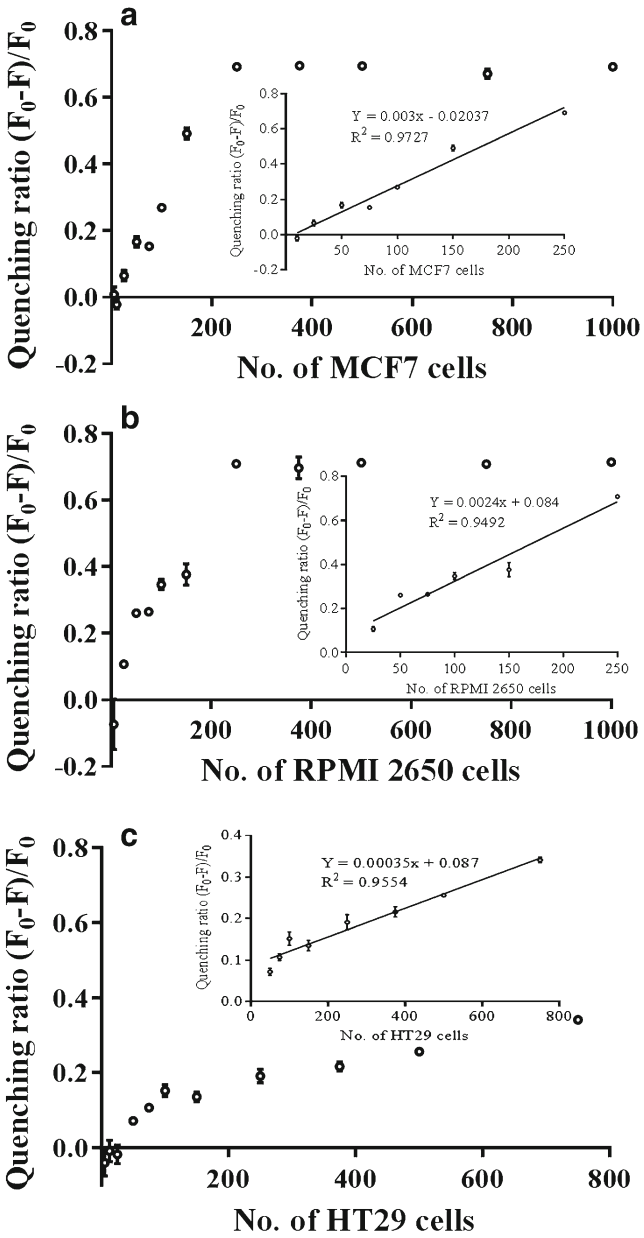

Fig. 4 Plots of quenching ratio with respect to different number of cells for (**a**) MCF7, (**b**) RPMI 2650 and (**c**) HT29. Insets show as the respective linear range of detection of different cell types. Error bars represent standard deviations of independent repeated measurements (n = 5)

This is evidenced from the characteristic signatures of positive bands at 210 and 260 nm, in addition to a less intense negative band at 240 nm. Comparatively, no characteristic positive band at 210 nm was observed for Ct_9TS and Ct_9TS-AgNCs, implying its B-form like structure [38]. Considering TRAP buffer contains additional components (e.g. EGTA and Tween 20) that may influence the optical properties of AgNCs, we have also investigated CD spectra of Ct_9TSR_n and Ct_9TSR_n-AgNCs prepared in Tris-HCl buffer (pH 8) for comparison (Fig. 5e and f). The CD results of Ct_9TSR_n templates in Tris-HCl buffer are generally similar to that in TRAP buffer. However, upon formation of AgNCs, Ct_9TSR_n-AgNCs in Tris-HCl demonstrate typical CD peaks of unfolded *G*-rich DNA [39–41].

TRAP buffer cannot be the main factor that is responsible for the fluorescence quenching, as Ct_9TS-AgNCs remained fluoresced. Thus, we postulate that the quenching effect observed in telomerase-positive samples is due to the formation of parallel *G*-quadruplexes. Noteworthy, in our previous study, samples with anti-parallel *G*-quadruplex (i.e. Apta5-AgNCs) showed relatively higher emission intensity than that of parallel topology (i.e. Apta3-AgNCs) [28]. This is also in accordance with the results reported by Tao et al., where parallel *G*-quadruplex has weaker fluorescence intensity than that with anti-parallel conformation. On top of *G*-quadruplex topology, thymine-rich loop bases adjacent to *G*-tetrads (i.e. *TTA* in this context) was also found to diminish the fluorescence signal [42]. At present, we do not fully understand how TRAP buffer contributes to the consistency of *G*-topology, both in Ct_9TSR_n-AgNCs containing different lengths of elongated products, as well as different telomerase cell extracts with varying degrees of telomerase activity. Note that an active telomerase is capable of elongating TS primer by hundreds of *TTAGGG* nucleotides through multiple rounds of repeat-addition [43, 44]. In comparison to those prepared in TRAP buffer, Ct_9TSR5- and Ct_9TSR7-AgNCs in Tris-HCl buffer show fluorescence enhancement, which is due to the proximity of *G*-rich tail that is known to increase the emission of adjacent AgNCs [45], similar as in NCB design. In contrast, the relatively shorter *G*-rich telomeric repeats of Ct_9TSR3 not only constraint their association with AgNCs hosted in Ct_9, but also undesirably disrupts the encapsulation of AgNCs.

Conclusion

A simple mix-and-detect assay for telomerase activity was successfully developed using Ct_9TS-AgNCs. We found that the probes were stable in cell extracts (tested up to 1000 cells) and showed selective quenching in different telomerase-positive cell extracts. A meticulous study on the quenching mechanism has shed important light on the impacts of *G*-quadruplexes topologies and buffer on the optical properties of AgNCs. Despite the assay is stable in cell extracts, its applicability in more complex matrices such as tissue samples requires careful investigations before clinical applications can be fully realized.

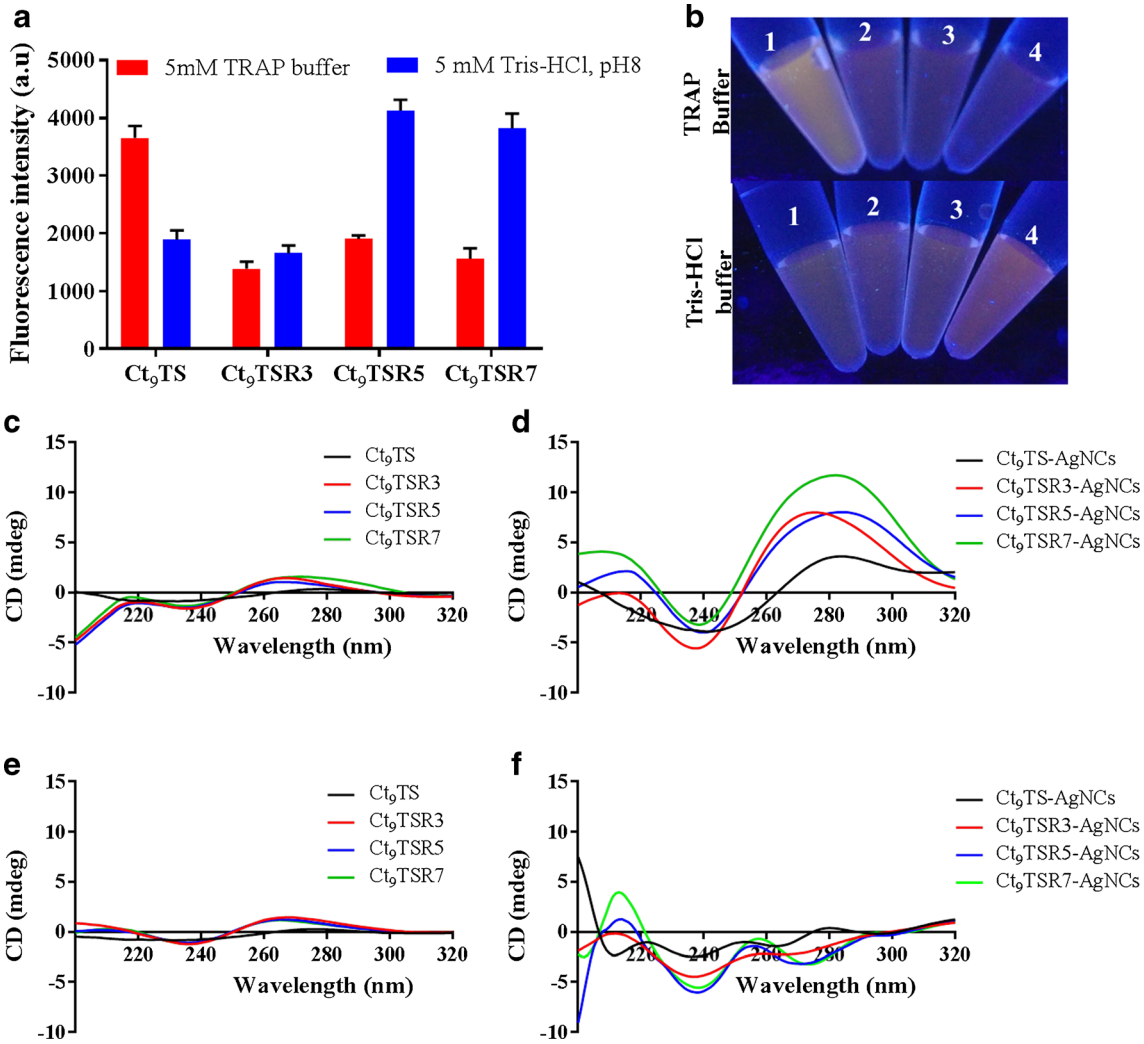

Fig. 5 **a** Fluorescence intensity of Ct_9TS and Ct_9TSRn-AgNCs, representing the absence and presence of different lengths of telomeric repeats, respectively. Each set of samples were prepared in two different buffers (i.e. TRAP and Tris-HCl) to study the effect of buffer. Error bars represent standard deviations from repeated independent measurements (n = 3). **b** The UV images of (1) Ct_9TS-, (2) Ct_9TSR3-, (3) Ct_9TSR5-, and (4) Ct_9TSR7-AgNCs. DNA concentration used for fluorescence measurement was 135 nM. CD spectra of Ct_9TS and Ct_9TSRn templates, as well as Ct_9TS-AgNCs and Ct_9TSRn-AgNCs prepared in (**c** & **d**) TRAP buffer and (e & f) Tris-HCl

Acknowledgements The authors would like to acknowledge Dr. Eunice Ngai and Rayan Sabra for supplying MCF7 and HT29, respectively. This work is supported by Fundamental Research Grant Scheme (FRGS) for financial support via FRGS/2/2014/SG06/UNIM/02/1.

Compliance with ethical standards

The author(s) declare that they have no competing interests.

References

1. Fleisig HB, Wong JMY (2007) Telomerase as a clinical target: current strategies and potential applications. Exp Gerontol 42: 102–112. https://doi.org/10.1016/j.exger.2006.05.011
2. Uziel O, Yosef N, Sharan R, Ruppin E, Kupiec M, Kushnir M, Beery E, Cohen-Diker T, Nordenberg J, Lahav M (2015) The effects of telomere shortening on cancer cells: a network model of proteomic and microRNA analysis. Genomics 105:5–16. https://doi.org/10.1016/j.ygeno.2014.10.013
3. Blackburn EH, Greider CW, Henderson E, Lee MS, Shampay J, Shippen-Lentz D (1989) Recognition and elongation of telomeres by telomerase. Genome 31:553–560. https://doi.org/10.1139/g89-104
4. Blackburn EH, Chan SRWL (2004) Telomeres and telomerase. Philos Trans R Soc Lond B 359:109–121. https://doi.org/10.1098/rstb.2003.1370
5. Blackburn EH (1991) Structure and function of telomeres. Nature 350:569–573. https://doi.org/10.1038/350569a0
6. Blackburn EH (2005) Telomeres and telomerase: their mechanisms of action and the effects of altering their functions. Federation of European Biochemical Societies Letters 579:859–862. https://doi.org/10.1016/j.febslet.2004.11.036
7. Blackburn EH (2005) Telomerase and Cancer: Kirk a. Landon–AACR prize for basic cancer research lecture. Mol Cancer Res 3: 477–482. https://doi.org/10.1158/1541-7786.MCR-05-0147

8. Kim NW, Piatyszek MA, Prowse KR, Harley CB, West MD, Ho PL, Coviello GM, Wright WE, Weinrich SL, Shay JW (1994) Specific association of human telomerase activity with immortal cells and cancer. Science 266:2011–2015. https://doi.org/10.1126/science/7605428
9. Zhang H, Wang Y, Wu M, Feng Q, Shi H, Chen HY, Xu JJ (2014) Visual electrochemiluminescence detection of telomerase activity based on multifunctional au nanoparticles modified with G-quadruplex deoxyribozyme and luminol. Chem Commun 50: 12575–12577. https://doi.org/10.1039/C4CC06302C
10. Meng F, Xu Y, Dong W, Tang Y, Miao P (2018) A PCR-free voltammetric telomerase activity assay using a substrate primer on a gold electrode and DNA-triggered capture of gold nanoparticles. Microchim Acta 185:398–404. https://doi.org/10.1007/s00604-018-2936-x
11. Ma C, Xia K, Chen H, Zeng W, Han R, Tang J (2012) Label-free highly sensitive detection of telomerase activity in cancer cell by chemiluminescence imaging. Mol Cell Probes 26:212–214. https://doi.org/10.1016/j.mcp.2012.06.002
12. Wang L, Zhang Y, Zhang C (2013) Ultrasensitive detection of telomerase activity at the single-cell level. Anal Chem 85:11509–11517. https://doi.org/10.1021/ac402747r
13. Wang J, Wu L, Ren J, Qu X (2014) Visual detection of telomerase activity with a tunable dynamic range by using a gold nanoparticle probe-based hybridization protection strategy. Nanoscale 6:1661–1666. https://doi.org/10.1039/c3nr05185d
14. Wang J, Wu L, Ren J, Qu X (2012) Visualizing human telomerase activity with primer-modified au nanoparticles. Small 8:259–264. https://doi.org/10.1002/smll.201101938
15. Yang Y, Li C, Hu X, Yang Y, Yin Y, Wang Z (2017) A programmed terminal extension strategy to light up multiple beacons for DNA and cellular telomerase detection. Chem Commun 53:5752–5755. https://doi.org/10.1039/C7CC02515G
16. Zheng G, Daniel WL, Mirkin CA (2008) A New approach to amplified telomerase detection with polyvalent oligonucleotide nanoparticle conjugates. J Am Chem Soc 130:9644–9645. https://doi.org/10.1021/ja803035p
17. Ding C, Li X, Ge Y, Zhang S (2010) Fluorescence detection of telomerase activity in cancer cells based on isothermal circular strand-displacement polymerization reaction. Anal Chem 82: 2850–2855. https://doi.org/10.1021/ac902818w
18. Wang H, Wu S, Chu X, Yu RQ (2012) A sensitive fluorescence strategy for telomerase detection in cancer cells based on T7 exonuclease-assisted target recycling amplification. Chem Commun 48:5916–5918. https://doi.org/10.1039/c2cc31878d
19. Zhang X, Cheng R, Shi Z, Jin Y (2016) A PCR-free fluorescence strategy for detecting telomerase activity via double amplification strategy. Biosens Bioelectron 75:101–107. https://doi.org/10.1016/j.bios.2015.08.013
20. Chen C, Wei M, Liu Y, Xu E, Wei W, Zhang Y, Liu S (2017) Visual and fluorometric determination of telomerase activity by using a cationic conjugated polymer and fluorescence resonance energy transfer. Microchim Acta 184:3453–3460. https://doi.org/10.1007/s00604-017-2362-5
21. Wang C, Wu J, Zong C, Xu J, Ju HX (2012) Chemiluminescent immunoassay and its applications. Chin J Anal Chem 40:3–10. https://doi.org/10.1016/S1872-2040(11)60518-5
22. Leung CH, Zhong HJ, Lu L, Chan DSH, Ma DL (2013) Luminescent and colorimetric strategies for the label-free DNA-based detection of enzyme activity. Briefing in Functional Genomics 12:525–535. https://doi.org/10.1093/bfgp/elt004
23. Syahir A, Usui K, Tomizaki K, Kajikawa K, Mihara H (2015) Label and label-free detection techniques for protein microarrays. Microarrays 4:228–244. https://doi.org/10.3390/microarrays4020228
24. Xu Y, Zhang P, Wang Z, Lv S, Ding C (2018) Determination of the activity of telomerase in cancer cells by using BSA-protected gold nanoclusters as a fluorescent probe. Microchim Acta 185:198–204. https://doi.org/10.1007/s00604-018-2734-5
25. Huang S, Yao H, Wang W, Zhang JR, Zhu JJ (2018) Highly sensitive fluorescent quantification of intracellular telomerase activity by repeat G-rich DNA enhanced silver nanocluster. J Mater Chem B 6: 4583–4591. https://doi.org/10.1039/C8TB00801A
26. Li X, Wang W, Yang D, Wu J, Zhang B, Wu Z, Tang J (2018) Telomerase activity detection in Cancer cell via primer extension-mediated fluorescence enhancement of silver nanoclusters. Anal Methods 10:2138–2143. https://doi.org/10.1039/C8AY00323H
27. Yeh H, Sharma J, Han JJ, Martinez JS, Werner JH (2010) A DNA - silver nanocluster probe that fluoresces upon hybridization. Nano Lett 1:3106–3110. https://doi.org/10.1021/nl101773
28. Lee ST, Beaumont D, Su XD, Muthoosamy K, New SY (2018) Formulation of DNA chimera templates: effects on emission behavior of silver nanoclusters and sensing. Anal Chim Acta 1010:62–68. https://doi.org/10.1016/j.aca.2018.01.012
29. Li J, Jia X, Li D, Ren J, Han Y, Xia Y, Wang E (2013) Stem-directed growth of highly fluorescent silver nanoclusters for versatile logic devices. Nanoscale 5:6131–6138. https://doi.org/10.1039/c3nr00998j
30. New SY, Lee ST, Su XD (2016) DNA-templated silver nanoclusters: structural correlation and fluorescence modulation. Nanoscale 8:17729–17746. https://doi.org/10.1039/C6NR05872H
31. Sengupta B, Ritchie CM, Buckman JG, Johnsen KR, Goodwin PM, Petty JT (2008) Base-directed formation of fluorescent silver clusters. J Phys Chem C 112:18776–18782
32. Yau SH, Abeyasinghe N, Orr M, Upton L, Varnavski O, Werner JH, Yeh HC, Sharma J, Shreve AP, Martinez JS, Goodson T (2012) Bright two-photon emission and ultra-fast relaxation dynamics in a DNA-templated nanocluster investigated by ultra-fast spectroscopy. Nanoscale 4:4247–4254. https://doi.org/10.1039/c2nr30628j
33. Hsu HC, Ho MC, Wang KH, Hsu YF, Chang CW (2015) DNA stabilized silver nanoclusters as the fluorescent probe for studying the structural fluctuations and the solvation dynamics of human telomeric DNA. New J Chem 39:2140–2145. https://doi.org/10.1039/C4NJ02065K
34. Yu J, Choi S, Dickson RM (2009) Shuttle-based fluorogenic silver-cluster biolabels. Angew Chem Int Ed 48:318–320. https://doi.org/10.1002/anie.200804137
35. Petty JT, Story SP, Juarez S, Votto SS, Herbst AG, Degtyareva NN, Sengupta B (2012) Optical sensing by transforming Chromophoric silver clusters in DNA Nanoreactors. Anal Chem 84:356–364
36. Ruttkay-Nedecky B, Skalickova S, Kremplova M, Nejdl L, Kudr J, Hynek D, Novotna M, Labuda J, Adam V, Kizek R (2014) Formation of G-quadruplex and its utilizing for an automated spectrometric detection of cisplatin. Int J Electrochem Sci 10:3973–3987
37. Lou X, Zhuang Y, Zuo X, Jia Y, Hong Y, Min X, Zhang Z, Xu X, Liu N, Xia F, Tang BZ (2015) Real-time, quantitative lighting-up detection of telomerase in urines of bladder Cancer patients by AIEgens. Anal Chem 87:6822–6827. https://doi.org/10.1021/acs.analchem.5b01099
38. Kypr J, Kejnovská I, Renčiuk D, Vorlíčková M (2009) Circular dichroism and conformational polymorphism of DNA. Nucleic Acids Res 37:1713–1725. https://doi.org/10.1093/nar/gkp026
39. Marchand A, Gabelica V (2016) Folding and misfolding pathways of G-quadruplex DNA. Nucleic Acids Res 44:10999–11012. https://doi.org/10.1093/nar/gkw970
40. Rehm C, Wurmthaler LA, Li Y, Frickey T, Hartig JS (2015) Investigation of a quadruplex-forming repeat sequence highly enriched in Xanthomonas and Nostoc sp. PLoS One 10:1–21. https://doi.org/10.1371/journal.pone.0144275

41. Jiang HX, Cui Y, Zhao T, Fu HW, Koirala D, Punnoose JA, Kong DM, Mao H (2015) Divalent cations and molecular crowding buffers stabilize G-triplex at physiologically relevant temperatures. Sci Rep 5:1–11. https://doi.org/10.1038/srep09255
42. Tao G, Chen Y, Lin R, Zhou J, Pei X, Liu F, Li N (2018) How G-quadruplex topology and loop sequences affect optical properties of DNA-templated silver nanoclusters. Nano Res 11:2237–2247. https://doi.org/10.1007/s12274-017-1844-4
43. Wu RA, Tam J, Collins K (2017) DNA-binding determinants and cellular thresholds for human telomerase repeat addition processivity. EMBO J 36:1908–1927. https://doi.org/10.15252/embj.201796887
44. Kelleher C, Teixeira MT, Klaus F, Lingner J (2002) Telomerase : biochemical considerations for enzyme and substrate. Trends Biochem Sci 27:572–579. https://doi.org/10.1016/S0968-0004(02)02206-5
45. Zhu J, Zhang L, Teng Y, Lou B, Jia X, Gu X, Wang E (2015) G-quadruplex enhanced fluorescence of DNA-silver nanoclusters and their application in bioimaging. Nanoscale 7:13224–13229. https://doi.org/10.1039/c5nr03092g